ELSEVIER

Journal of Biomechanics 36 (2003) 873–882

JOURNAL OF BIOMECHANICS

www.elsevier.com/locate/jbiomech
www.JBiomech.com

A new model-based RSA method validated using CAD models and models from reversed engineering

B.L. Kaptein[a,*], E.R. Valstar[a], B.C. Stoel[b], P.M. Rozing[a], J.H.C. Reiber[b]

[a] *Department of Orthopaedics, Leiden University Medical Center, P.O. Box 9600 RC, Leiden 2300, The Netherlands*
[b] *Department of Radiology, Division of Image Processing, Leiden University Medical Center, P.O. Box 9600 RC, Leiden 2300, The Netherlands*

Abstract

Roentgen stereophotogrammetric analysis (RSA) was developed to measure micromotion of an orthopaedic implant with respect to its surrounding bone. A disadvantage of conventional RSA is that it requires the implant to be marked with tantalum beads. This disadvantage can potentially be resolved with model-based RSA, whereby a 3D model of the implant is used for matching with the actual images and the assessment of position and rotation of the implant. In this study, a model-based RSA algorithm is presented and validated in phantom experiments. To investigate the influence of the accuracy of the implant models that were used for model-based RSA, we studied both computer aided design (CAD) models as well as models obtained by means of reversed engineering (RE) of the actual implant.

The results demonstrate that the RE models provide more accurate results than the CAD models. If these RE models are derived from the very same implant, it is possible to achieve a maximum standard deviation of the error in the migration calculation of 0.06 mm for translations in x- and y-direction and 0.14 mm for the out of plane z-direction, respectively. For rotations about the y-axis, the standard deviation was about 0.1° and for rotations about the x- and z-axis 0.05°. Studies with clinical RSA-radiographs must prove that these results can also be reached in a clinical setting, making model-based RSA a possible alternative for marker-based RSA.

Keywords: RSA; Pose estimation; Model-based; Roentgen stereophotogrammetry

1. Introduction

In total joint arthroplasty, fixation of the implant in the surrounding bone is of greatest importance for the success of the procedure. To study the fixation of implants, roentgen stereophotogrammetric analysis (RSA) was developed by Selvik in 1974 (Selvik, 1989). With this accurate three-dimensional measurement technique, micromotion between the implant and the surrounding bone can be assessed in an early stage (Nagels et al., 2002; Valstar et al., 2002; Nelissen et al., 1998; Ryd, 1992; Selvik, 1989). The reported accuracy of RSA ranges between 0.05 and 0.5 mm for translations and between 0.15° and 1.15° for rotations (95% confidence interval; (Kärrholm, 1989; Valstar et al., 2000).

To guarantee the high accuracy of RSA, it has been necessary until today to mark the implant and the surrounding bone with tantalum beads. From the projections of these markers, detected in a stereo-pair of roentgen images, their three-dimensional (3-D) positions are reconstructed, resulting in an accurate calculation of the pose of the bone and the implant (Börlin et al., 2002; Valstar et al., 2000; Vrooman et al., 1998).

One of the major difficulties and disadvantages of RSA is that the marking of the implants drastically increases the costs of the implants and lengthens the start-up period of an RSA study. It is also possible that marking the implant jeopardizes the strength of the implant, and the markers may also cause local stress raisers in the bone cement resulting in cement cracks that may jeopardize the strength of the fixation of the implant in the bone. Another problem is that the markers, which are attached to the implant, are often overprojected by the implant itself.

*Corresponding author. Tel.: +31-71-526-4542; fax: +31-71-526-6743.
E-mail address: b.l.kaptein@lumc.nl (B.L. Kaptein).

0021-9290/03/$ - see front matter
doi:10.1016/S0021-9290(03)00002-2

To avoid the requirement of using markers on the implant for RSA, a model-based RSA method was developed (Valstar et al., 2001; Jong, 1997). This technique is based on minimizing the difference between the virtual projection of a 3-D surface model of an implant with the actual projection of the implant as it appears in a roentgen image. If the implant is a non-symmetric object, its projection is unique in most instances. Therefore, the pose of an implant can be estimated from its projection by finding the corresponding pose of the model of this implant, such that minimal differences remain. This technique originates from 3-D vision (Wunsch and Hirzinger, 1996; Lowe, 1987) and is also used in Roentgen Fluoroscopic Analysis. (Guéziec et al., 2000; Zuffi et al., 1999; Sarojak et al., 1999; Hoff et al., 1998; Banks and Hodge, 1996; Lavallée and Szeliski, 1995).

In a pilot study carried out at our department (Valstar et al., 2001), the non overlapping area (NOA) approach was used as a measure of the difference between the actual projection and the virtual projection. It was concluded that the established accuracy of conventional marker-based RSA could not be reached with this specific approach for model-based RSA due to the relatively large dimensional differences between the computer aided design (CAD) model of the implant and the actual implant. To overcome this problem, it became clear that it is necessary to remove the unreliable parts of the contours originating from inaccurate parts of the model. These "drop-outs" in the contours are also generated in the case of a partial overlap of the projections of different prosthetic components.

Because the NOA method cannot handle contours that contain drop-outs, we have developed an improved model-based RSA algorithm that can handle contours that contain drop-outs. This algorithm was tested in model simulation experiments and it was shown that theoretically the improved algorithm would be able to accurately determine the pose of the implant. The promising results of these simulation experiments have stimulated us to validate the improved algorithm in phantom experiments.

The aim of the present study is, therefore, to validate the improved model-based RSA algorithm in phantom experiments and to investigate the effect of using either CAD models or models from reversed engineering.

2. Material

2.1. RSA set-up

In this study, an RSA set-up was used that contained two synchronized roentgen tubes positioned at approximately 1.5 m above the film cassette. Each roentgen tube was directed towards one half of the roentgen film at an angle of 20° relative to the normal vector of the roentgen film. A carbon calibration box with 1-mm tantalum markers was positioned underneath the roentgen table. This calibration box defines the laboratory coordinate system and is used to accurately calculate the positions of the roentgen foci. In the laboratory coordinate system, the x-axis is defined inside the image plane parallel to the line connecting the two foci. The y-axis is defined inside the image plane perpendicular to the x-axis and the z-axis is defined perpendicular to the image plane. Fig. 1 shows the RSA-CMS software with an RSA image showing the phantom that was used in this study, calibration markers, and the laboratory coordinate system.

2.2. Models and components

In this validation study the femoral and tibial components of the Interax total knee prosthesis (Stryker Howmedica Osteonics Corp., Rutherfort, USA) were used. The implant manufacturer provided two femoral components and two tibial components of the same size and type. CAD models of both corresponding components were also provided. These CAD models were converted to triangulated surface models using the MSC/PATRAN software package (Mac-Neal-Schwendler GmbH, Munich, Germany). The model of the femoral component consisted of 3600 elements and the tibial model of 6290 elements. For the remainder of this manuscript, we will refer to these models as CAD models.

One of the femoral components and one of the tibial components were also laser scanned, producing reversed engineered (RE) models of 252978 and 571920 elements, respectively. The accuracy of this reversed engineering technique is 0.013 mm.The prosthetic components that were used to generate the RE models are denoted: scanned components. The other components are denoted non-scanned components.

2.3. Phantom

The phantom consisted of the femoral or tibial component rigidly clamped inside a small carbon box in which 17 beads were attached to the edges. This phantom box was used in two different experiments: In the first experiment, it was possible to accurately translate the phantom box in x- and z-directions with respect to the calibration box by means of a calibrated micromanipulator attached to the calibration box (accuracy 0.005 mm).

In the second experiment another construction was used to rotate the phantom box in reproducible poses with respect to the calibration box.

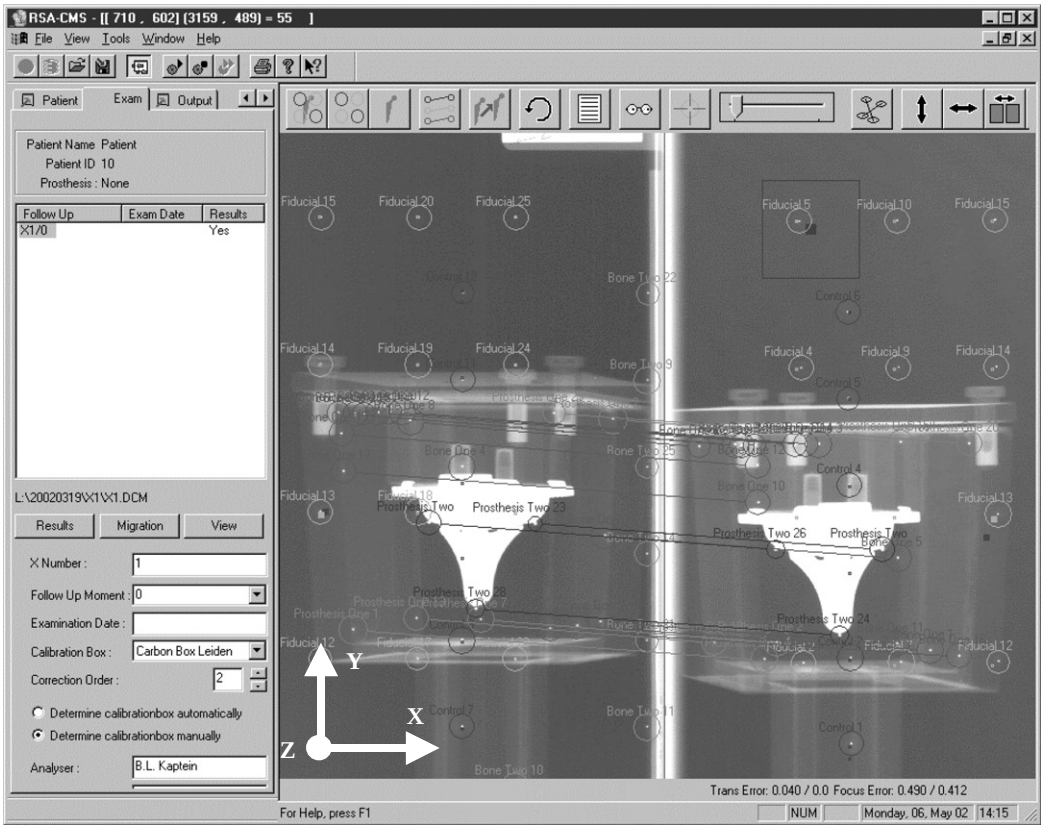

Fig. 1. RSA-CMS software showing part of an RSA image of the phantom with tibia component clamped inside and the laboratory axis system. All RSA markers are detected and labelled. The connection lines of the phantom and tibia markers are also shown. In the lower left corner, the laboratory axis system is shown.

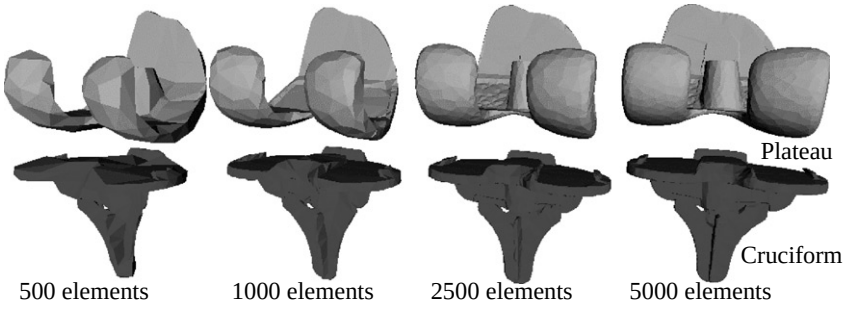

Fig. 2. The RE models that have been used in this study. Note that the tibia component is a constellation of a plateau and a cruciform part.

3. Method

3.1. Model reduction

For each component, less detailed RE models were constructed by reducing the original RE model to 5000, 2500, 1000, and 500 triangular elements, respectively (Fig. 2). This was not only necessary for obtaining an acceptable calculation time, but also to establish the relation between the number of triangular elements of the model and the accuracy of the method. Therefore we repeated all calculations using the CAD-models and these reduced RE-models.

3.2. Contour detection and model projection

The actual contour of the implant in the radiograph was detected by means of the Canny operator (Canny, 1986). A human operator interactively removed those parts of the contour that were clearly not part of the boundary of the projection of the implant. This removal usually takes less than a minute time of the operator and no special skills of the operator are necessary. Note that the contour can consist of multiple contour parts that do not necessarily form a closed contour.

By means of computer graphic techniques, the 3-D model of the implant was projected onto the image

plane and a virtually projected contour was calculated (Valstar et al., 2001). In contrast to the detected contour, the calculated virtual contour is a closed contour. The virtual contour can be described as a function of the model, the pose of the model, and the position of the focus:

$$\text{Virtual Contour} = \text{F(Model, Model Pose, Focus)}. \quad (1)$$

3.3. Contour difference

We define the actual contour and the virtual contour as a chain of nodes:

$$\text{Actual Contour}: A_i = (x, y, z) \qquad (i = 1 - n_A), \quad (2)$$

$$\text{Virtual Contour}: V_j = (x, y, z) \qquad (j = 1 - n_v), \quad (3)$$

in which n_A is the number of nodes in the actual contour and n_V is the number of nodes in the virtual contour. Note that because the xy-plane of the coordinate system is defined as the projection plane of the roentgen system, all z-coordinates of the projection contours are zero. The difference between the actual contour and the virtual contour is defined as the mean distance between the nodes of the actual contour and the virtual contour:

$$\text{DIF} = F(\text{Actural Contour, Virtual Contour}) = \sum_{i=1-n_A} ||A_i - A_i^p||/n_A$$

in which A_i^p is the closest projection of node i of the actual contour onto the virtual contour (Fig. 3).

3.4. Minimisation of the contour difference

In order to calculate the three-dimensional position and orientation of the implant, the contour difference between the actual contour and the virtual contour must be minimised. To accomplish this, first the pose of the implant was set interactively by a human operator. Secondly, an iterative inverse perspective matching (IIPM) algorithm was used. This algorithm is based on the work of Wunsch and the iterative closest point (ICP) algorithm of Besl (Wunsch and Hirzinger, 1996; Besl and McKay, 1992). For the final accurate pose estimation, we used a minimisation algorithm that minimises the objective function, which is composed of the differences between the virtual and actual contour from the left and right image halve:

$$\text{DIF} = \text{DIF}_{\text{LEFT}} + \text{DIF}_{\text{RIGHT}} \quad (5)$$

with

$$\text{DIF}_{\text{LEFT}} = F(\text{Actual Contour}_{\text{LEFT}}, \text{Virtual Contour}_{\text{LEFT}}), \quad (6)$$

$$\text{DIF}_{\text{RIGHT}} = F(\text{Actual Contour}_{\text{RIGHT}}, \text{Virtual Contour}_{\text{RIGHT}}). \quad (7)$$

In this objective function, the virtual contour is a function of the model pose (1). The model pose, that consists of the three position coordinates and three orientation parameters, is the only unknown in the objective function. For minimisation of this highly non-linear function, a sequential quadratic programming (SQP) minimization scheme is used, as described by Spellucci (Spellucci, 1998). In this scheme, the partial derivative of the objective function is calculated using a finite difference method. See Fig. 4 for a detail of the actual contour and the matched virtual contour. This figure also shows an overview of the model with its projection. A similar approach was used in a single focus set-up by Fukuoka (Fukuoka et al., 1999).

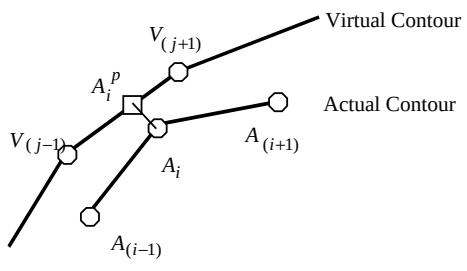

Fig. 3. Closest connection line between point A_i of the actual contour, and its projection point on the virtual contour.

4. Phantom Experiment I: small translations

4.1. Experimental set-up

To test the accuracy of the improved model-based RSA techniques with different models, the phantom was positioned in seven successive poses and an RSA radiograph was acquired in each pose. By means of the micromanipulator, which is considered as a gold-standard for setting a position with respect to the calibration box, the phantom was translated over a distance of 1.0 mm alternatively in the x- and z-directions between the successive poses with a maximum displacement of 3 mm in each direction. Translations in the y-direction and rotations were not applied. The position and orientation of the implant were assessed by means of the model-based RSA algorithm. By using its attached markers, the position and orientation of the phantom box could be assessed with marker-based RSA. In each measurement, the pose of the phantom box and the implant were calculated separately. We subtracted the succeeding calculated poses from each other and compared this calculated motion between the successive radiographs with the actual motion as was applied by the micromanipulator. The standard deviation of the differences between these calculated motions and the actual motions is a measure for the accuracy of

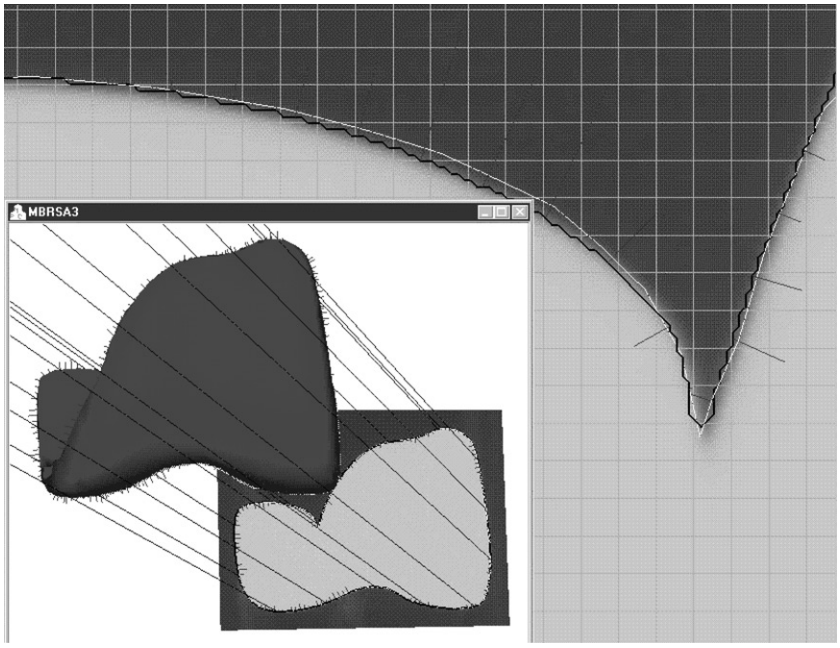

Fig. 4. Detail of the roentgen image with the actual detected contour (black) and the matched virtual contour (white). The size of the grid that is shown in this image is 1 mm and the short lines perpendicular to the contours is a ten times the enlargement of the shortest lines connecting the actual and the virtual contour. The inserted figure shows an overview of the model and one of the complete projections.

Table 1
Mean and standard deviation (SD) of the difference between calculated and applied motion of the scanned femur component (n=6)[a]

Model		DIF	x	y	z	R_x	R_y	R_z
CAD	Mean	0.22	−0.003	−0.009	−0.011	−0.022	−0.001	0.001
3600 el.	SD	0.01	0.025	0.038	0.150	0.090	0.119	0.051
RE	Mean	0.38	−0.003	−0.010	−0.018	−0.002	0.037	0.008
500 el.	SD	0.01	0.031	0.040	0.132	0.038	0.081	0.024
RE	Mean	0.15	−0.001	−0.011	−0.019	−0.006	0.036	0.006
1000 el.	SD	0.01	0.034	0.032	0.148	0.054	0.049	0.048
RE	Mean	0.07	−0.003	−0.006	−0.017	−0.002	0.012	0.001
2500 el.	SD	0.00	0.029	0.027	0.148	0.080	0.045	0.063
RE	Mean	0.05	−0.004	−0.006	−0.019	0.000	0.017	0.000
5000 el.	SD	0.01	0.028	0.029	0.147	0.067	0.044	0.058
Marker-	Mean	—	−0.002	0.005	0.023	0.000	0.001	−0.003
Based	SD	—	0.014	0.026	0.073	0.022	0.036	0.015

In this experiment, the very same femur component was also used to generate the RE-model.

[a] DIF = Mean distance between the nodes of the actual contour and the virtual contour. Translations are labelled x, y, and z (in mm) and rotations are labelled R_x, R_y, and R_z (in deg).

the pose estimation algorithm, the mean of these differences is also presented in this paper because it shows that the algorithm has no systematic errors.

4.2. Results

Tables 1–4 show the results for this experiment. To compare the results of model-based RSA with the results of marker-based RSA in this experiment, the last row in these tables shows the results for marker-based RSA. Especially for the orientation, marker-based RSA is more accurate than model-based RSA.

The results for model-based RSA show that for the scanned femur component (Table 1), the standard deviation of the x- and y-component of the measured motion difference is less than 0.04 mm for all tested models. The standard deviation of the out-of-plane z-component of the motion difference is about 0.15 mm.

Table 2
Mean and standard deviation (SD) of the difference between calculated and applied motion of the non-scanned femur component (n=6)[a]

Model		DIF	x	y	z	R_x	R_y	R_z
CAD	Mean	0.21	0.003	0.020	−0.027	0.040	0.020	0.014
6290 el.	SD	0.01	0.078	0.041	0.277	0.033	0.079	0.158
RE	Mean	0.13	0.002	0.015	−0.024	0.023	−0.018	0.011
2500 el.	SD	0.00	0.039	0.046	0.206	0.041	0.015	0.020
Marker-	Mean	—	−0.002	−0.005	−0.004	−0.007	0.004	−0.002
Based	SD	—	0.018	0.028	0.111	0.025	0.031	0.006

In this experiment, another same femur component was also used to generate the RE-model.
[a] DIF = Mean distance between the nodes of the actual contour and the virtual contour. Translations are labelled x, y, and z (in mm) and rotations are labelled R_x, R_y, and R_z (in deg).

Table 3
Mean and Standard Deviation (SD) of the difference between calculated and applied motion of the scanned tibia component (n=6)[a]

Model		DIF	x	y	z	R_x	R_y	R_z
CAD	Mean	0.37	−0.006	0.001	0.043	−0.004	−0.003	0.021
6290 el.	SD	0.00	0.041	0.026	0.080	0.091	0.117	0.058
RE	Mean	0.42	0.003	0.005	0.034	−0.018	−0.052	0.002
500 el.	SD	0.06	0.249	0.143	0.780	0.125	0.147	0.217
RE	Mean	0.16	0.003	0.001	0.035	−0.015	−0.015	0.000
1000 el.	SD	0.00	0.040	0.031	0.077	0.106	0.028	0.021
RE	Mean	0.08	0.002	−0.003	0.031	−0.017	−0.011	0.005
2500 el.	SD	0.00	0.037	0.023	0.080	0.123	0.076	0.031
RE	Mean	0.06	0.002	−0.003	0.036	−0.017	−0.021	0.006
5000 el.	SD	0.00	0.040	0.019	0.080	0.118	0.057	0.027
Marker-	Mean	—	0.011	−0.002	−0.026	−0.003	0.002	−0.005
based	SD	—	0.031	0.019	0.073	0.034	0.014	0.016

In this experiment, the very same tibia component was also used to generate the RE-model.
[a] DIF = Mean distance between the nodes of the actual contour and the virtual contour. Translations are labelled x, y, and z (in mm) and rotations are labelled R_x, R_y, and R_z (in deg).

Table 4
Mean and standard deviation (SD) of the difference between calculated and applied motion of the non-scanned tibia component (n=6)[a]

Model		DIF	x	y	z	R_x	R_y	R_z
CAD	Mean	0.20	0.008	−0.003	0.027	0.025	0.011	−0.005
6290 el.	SD	0.01	0.066	0.077	0.070	0.094	0.164	0.093
RE	Mean	0.29	−0.001	−0.007	−0.007	0.013	−0.033	−0.009
2500 el.	SD	0.01	0.090	0.057	0.097	0.170	0.137	0.037
Marker-	Mean	—	0.003	−0.011	0.005	-0.009	0.002	0.002
based	SD	—	0.032	0.023	0.110	0.040	0.042	0.027

In this experiment, another same tibia component was also used to generate the RE-model.
[a] DIF = Mean distance between the nodes of the actual contour and the virtual contour. Translations are labelled x, y, and z (in mm) and rotations are labelled R_x, R_y, and R_z (in deg).

For the orientation, the standard deviation is less than 0.081° for all orientation parameters. For the RE model fitted on the non-scanned femur component (Table 2), the out of plane z-component of the motion difference is about 0.2 mm, but the standard deviations of the measured rotation differences are less than 0.04°.

For the scanned tibia component (Table 3), there is a drop in the accuracy in the situation where the number of triangular elements equals 500; however if the model contains more than 1000 elements, the accuracy is even better than the accuracy obtained for the femoral component.

Table 5
Mean and standard deviation (SD) of the migration of the scanned femur component with respect to the phantom box (n=8)[a]

Model		DIF	x	y	z	R_x	R_y	R_z
CAD	Mean	0.22	0.028	−0.026	0.053	−0.022	−0.052	0.056
3600 el.	SD	0.02	0.155	0.080	0.283	0.289	0.278	0.150
RE	Mean	0.39	0.022	0.006	−0.088	0.197	0.047	0.024
500 el.	SD	0.01	0.185	0.111	0.387	0.203	0.586	0.490
RE	Mean	0.16	−0.024	0.012	−0.047	0.080	0.023	0.026
1000 el.	SD	0.01	0.068	0.048	0.148	0.101	0.165	0.119
RE	Mean	0.07	−0.035	0.012	−0.030	0.008	0.022	0.002
2500 el.	SD	0.01	0.047	0.039	0.147	0.063	0.127	0.055
RE	Mean	0.05	−0.033	0.010	−0.030	−0.004	0.011	0.008
5000 el.	SD	0.00	0.047	0.045	0.138	0.058	0.104	0.027
Marker-	Mean	—	0.022	−0.000	−0.002	−0.013	0.018	−0.021
based	SD	—	0.049	0.031	0.079	0.067	0.065	0.044

In this experiment, the very same femur component was used to generate the RE-model.
[a] DIF = Mean distance between the nodes of the actual contour and the virtual contour. Translations are labelled x, y, and z (in mm) and rotations are labelled R_x, R_y, and R_z (in deg).

Table 6
Mean and standard deviation (SD) of the migration of the non-scanned femur component with respect to the phantom box (n=8)[a]

Model		DIF	x	y	z	R_x	R_y	R_z
CAD	Mean	0.22	0.054	−0.012	0.027	−0.040	0.005	0.104
3600 el.	SD	0.01	0.133	0.089	0.288	0.331	0.146	0.133
RE	Mean	0.13	−0.007	0.003	0.011	−0.015	0.047	0.039
2500 el.	SD	0.01	0.074	0.050	0.080	0.068	0.275	0.056
Marker-	Mean	—	0.011	0.005	0.001	0.006	0.022	−0.004
based	SD	—	0.033	0.030	0.050	0.045	0.057	0.040

In this experiment, another femur component was used to generate the RE-model.
[a] DIF = Mean distance between the nodes of the actual contour and the virtual contour. Translations are labelled x, y, and z (in mm) and rotations are labelled R_x, R_y, and R_z (in deg).

In Table 3, we see that the results of the CAD model are similar to the results of the RE model. For the non-scanned tibia component (Table 4), the results are almost similar to the results of the scanned tibia component.

5. Phantom experiment II: larger rotations

5.1. Experimental set-up

In a second phantom experiment, the phantom was positioned in nine standardised poses within a range of knee poses we have encountered during our clinical RSA studies (0–10–20° exo-rotation in all possible combinations with 0–10–20° flexion). Because the centre of these rotations was external to the phantom, these rotations also changed the position of the phantom with respect to the calibration box. In this experiment, the model-based RSA algorithm was tested against the marker-based RSA algorithm by calculating the migration between the implant and the markers in the phantom box.

Since the implant is rigidly clamped inside this box, there is no change in relative pose between the implant and the markers of the phantom box in between the successive radiographs. Thus the migration that we measure between the implant and the markers in the phantom box is a measure for the error of the model-based RSA algorithm. To test the accuracy of marker-based RSA in these experiments, the markers in the phantom box were divided into two groups and the migration between these two marker groups in between two successive radiographs was calculated.

5.2. Results

Tables 5–8 show the results of the second phantom experiment as the mean and standard deviation of the

Table 7
Mean and standard deviation (SD) of the migration of the scanned tibia component with respect to the phantom box (n=8)[a]

Model		DIF	x	y	z	R_x	R_y	R_z
CAD	Mean	0.36	0.025	−0.039	−0.095	−0.112	0.142	0.014
6290 el.	SD	0.01	0.128	0.148	0.130	0.508	1.422	0.370
RE	Mean	0.32	0.066	−0.005	0.085	0.037	0.150	0.129
500 el.	SD	0.05	0.068	0.073	0.416	0.253	1.021	0.236
RE	Mean	0.16	0.025	0.006	0.052	0.026	0.093	0.068
1000 el.	SD	0.03	0.092	0.070	0.153	0.216	0.855	0.182
RE	Mean	0.08	0.012	0.000	0.030	−0.008	0.058	0.041
2500 el.	SD	0.02	0.070	0.054	0.076	0.134	0.323	0.109
RE	Mean	0.06	0.001	0.001	0.012	−0.005	0.024	0.024
5000 el.	SD	0.00	0.062	0.060	0.088	0.089	0.172	0.045
Marker-	Mean	—	0.012	−0.005	0.014	0.012	−0.002	−0.003
based	SD	—	0.023	0.015	0.051	0.054	0.055	0.025

In this experiment, the very same tibia component was used to generate the RE-model.
[a] DIF = Mean distance between the nodes of the actual contour and the virtual contour. Translations are labelled x, y, and z (in mm) and rotations are labelled R_x, R_y, and R_z (in deg).

Table 8
Mean and standard deviation (SD) of the migration of the non-scanned tibia component with respect to the phantom box (n=8)[a]

Model		DIF	x	y	z	R_x	R_y	R_z
CAD	Mean	0.23	0.008	0.018	−0.019	0.113	−0.179	−0.070
6290 el.	SD	0.03	0.209	0.123	0.103	0.386	0.811	0.680
RE	Mean	0.28	−0.020	0.053	−0.038	−0.021	−0.121	−0.039
2500 el.	SD	0.02	0.202	0.088	0.211	0.361	1.256	0.338
Marker-	Mean	—	0.017	−0.008	0.025	0.000	−0.009	−0.014
based	SD	—	0.044	0.025	0.071	0.057	0.053	0.020

In this experiment, another tibia component was used to generate the RE-model.
[a] DIF = Mean distance between the nodes of the actual contour and the virtual contour. Translations are labelled x, y, and z (in mm) and rotations are labelled R_x, R_y, and R_z (in deg).

calculated migration. The last rows in these tables demonstrate that for this experiment, marker-based RSA is more accurate than model-based RSA and can be used as a gold standard to validate the improved model-based RSA algorithm. The mean values of the calculated migration of both the model-based RSA as well as the marker-based RSA were low relative to the standard deviation. For model-based RSA, the standard deviation of the x- and y-component of the measured translation is less than 0.05 mm when using a model of 5000 elements for the scanned femur component (Table 5). For the out-of-plane z-translation, the standard deviation is about 0.14 mm.For the measured rotation, the standard deviation reaches a maximum of about 0.1° for the R_y_component. Note, that for the non-scanned femur component in Table 6, the standard deviation for translations in the z-direction is smaller than for the scanned femur component (0.09 mm), but the standard deviation for the rotation about the y-axis is relatively large (0.28°).

For the CAD model, the accuracy of both the scanned and the non-scanned femoral components is the same. The largest standard deviation for the translations is about 0.3 mm for the z-translation and for the rotations about 0.3° for rotations about the x-axis.

For the scanned tibia component, the standard deviation is about 0.06 mm for x- and y-translations and 0.09 mm for translations in the out-of-plane z-direction (Table 7). For rotations, the largest standard deviation is 0.17° for rotations about the y-axis and about 0.09 and 0.05° for rotations about the x- and z-axis, respectively. Note that for the non-scanned tibia component (Table 8), the standard deviations are relatively large compared to the standard deviations of Table 7. These results show that for the tibia component, the difference between the scanned and non-scanned component is much larger than for the femoral component.

For the CAD model there is again not really a difference between the scanned and non-scanned tibia

component. The largest standard deviation of the translation parameters is about 0.2 mm and for the rotation parameters even 1.4°.

6. Discussion

The goal of this study was to validate the new model-based RSA algorithm and to investigate the effect of using either CAD models or models from reversed engineering.

When we study the differences between the results of experiments I and II, the following conclusions can be drawn: In experiment I, where only small translations are applied, the difference between the results using the CAD model and the results using the RE model is smaller than in experiment II. Also the difference in results between the scanned and non-scanned components in experiment I is smaller than in experiment II. The results also demonstrate that the relationship between the difference measure and the accuracy of the pose estimation is stronger in experiment II than in experiment I.

We believe that this relatively high accuracy for less accurate models, such as the non-scanned components and the CAD models, in experiment I, is caused by the small displacements of the phantom between the different radiographs in this experiment. These small displacements make that the differences between the projections are also small. A shape difference between the model and the actual implant will show-up the same in each radiograph, and thus cause the same error in pose estimation for each radiograph.

From this phenomenon, we conclude that for phantom experiments, where we need high sensitivity for model-component differences to test the algorithms, it is important that the phantom is placed in different positions and orientations within the clinical range. In clinical experiments, where we require low sensitivity for model-component differences, the patient should be positioned as well as possible the same for each radiograph.

The differences between the results of experiment I and experiment II are even stronger for the tibia component. This is caused by the fact that the tibia component is a constellation of a cruciform stem and a plateau. The relative position between these two parts is not uniquely defined, resulting in larger differences between the different tibia components.

In general, we see that when RE models are used, the results are always superior to the results for CAD models, even when a non-scanned component is used. This implies that the difference between the CAD model and a component is larger than the difference between the components themselves. So one of the important things we showed in this paper is that one should not assume that a CAD model as provided by the manufacturer is the best model for model-based RSA without doing some tests. We realise that in this paper, this is only tested for this specific implant, but in general we think that for model-based RSA, an RE model is always better, or equally good as a CAD model.

Great advantages of the presented algorithm are that it has no systematic errors, as were found in the study of Valstar et al. (Valstar et al. 2001) and it can handle contours that contain drop-outs.

When we compare the results presented in this paper with the results obtained by Valstar et al. (Valstar et al., 2001), who also used the Interax knee prosthesis, the following observations can be made: For the CAD models, the standard deviation for translations in the x- and y-direction in this study is similar to the results in the study of Valstar, but the standard deviation of the translations in the z-direction is larger in this study (0.29 mm compared to 0.17 mm). For rotations, the study of Valstar shows a standard deviation of about 0.5° around the y-axis compared to a maximum of about 0.3° in this study. For the mean values, this study has a maximum 0.05 mm for translations in the x-direction, and 0.1° for rotations around the z-axis, while Valstar found a maximum of −0.10 mm for translations in z-direction and 0.26° for rotations around the y-axis.

For the tibia component, the CAD model that was used in this study was not exactly the same as the CAD model that was used in the study of Valstar because the relative position and orientation between stem and plateau of the model was different. This might be the cause that the standard deviations for the CAD model are larger in this study compared to the study of Valstar, but the mean values are smaller.

Therefore, we can conclude that the improvements of the algorithm show-up for the most part in the reduction of the mean values (systematic errors), and that the improved algorithm also works with incomplete contours.

Because other research groups only tested their algorithms in single focus experiments, it is difficult to compare our results with their results. But when we do, we see that Banks and Hodge calculated, by means of fluoroscopy, the relative motions between a femoral and a tibia component in an in vitro experiment. They published standard errors of 0.19, 0.14, and 3.90 mm for x, y, and z translations, respectively. For the rotations, they found standard errors of 1.3°, 1.2°, and 1.1° around the x-, y- and z-axis, respectively (Banks and Hodge, 1996).

Fukuoka et al. used single focus X-ray images to calculate wear in a total knee prosthesis. They presented results for an in vitro study with maximum standard deviations for translations of 0.09 mm in-plane and 0.87 mm out-of-plane, and for rotations 0.08° in-plane and 0.13° out-of-plane (Fukuoka et al., 1999).

We observe, as was to be expected, that with stereo images, the out-of-plane translation can be estimated far better than with single focus images. In a future study, we will also test our algorithm in a single focus set-up.

Compared to marker-based RSA, we see that the accuracy of model-based RSA is always lower. We think that by slightly increasing the number of patients included in a clinical trial, it is possible to reach the same power as marker-based RSA.

7. Conclusion

In this paper we have presented an improved model-based RSA algorithm and tested it in phantom experiments. This work demonstrates that using models obtained by reversed engineering of actual components provides accurate results, as opposed to using CAD models. We showed that if the RE-models are derived from the very same prosthetic component, it is possible to achieve a standard deviation of the error in the migration calculation that stays within 0.06 mm for translations in x- and y-directions and 0.14 mm for the out of plane z-direction, respectively. For the rotations, the largest standard deviation was about 0.1° for rotations about the y-axis and 0.05° for rotations about the x- and z-axis, respectively. For the femur component, it was also possible to reach accurate results for non-scanned components. For the tibia component, this was not possible because of the larger differences between the different tibia components.

Studies with clinical RSA-radiographs must prove that these results can also be reached in a clinical setting, making model-based RSA a possible, but less accurate, alternative for marker-based RSA to study the migration of prostheses.

Acknowledgements

The authors are very grateful to MEDIS medical imaging systems B.V. and the Technology Foundation STW for their financial support of this project.

The authors are also very grateful to Howmedica for providing the CAD models and prosthetic components, TNO Industry for providing the RE models of the prosthetic components, and to Eric Garling for the assistance with making the RSA radiographs.

References

Banks, S.A., Hodge, W.A., 1996. Accurate measurement of three-dimensional knee replacement kinematics using single-plane fluoroscopy. IEEE Transactions on Biomedical Engineering 43, 638–649.

Besl, P.J., McKay, N.D., 1992. A method for registration of 3-D shapes. IEEE Transactions on PAMI 14, 239–256.

Börlin, N., Thien, T., Kärrholm, J., 2002. The precision of radiostereometric measurements. Manual vs. digital measurements. Journal of Biomechanics 35, 69–79.

Canny, 1986. A computational approach to edge detection. IEEE Transactions on PAMI 8, 679–698.

Fukuoka, Y., Hoshino, A., Ishida, A., 1999. A simple radiographic measurement method for polyethylene wear in total knee arthroplasty. IEEE Transactions on Rehabilitation Engineering 7, 228–233.

Guéziec, A., Wu, K., Kalvin, A., Williamson, B., Kazanzides, P., Van Vorhis, R., 2000. Providing visual information to validate 2-D to 3-D registration. Medical Image Analysis 4, 357–374.

Hoff, W.A., Komistek, R., Dennis, D.A., Gabriel, S.M., Walker, S.A., 1998. Three-dimensional determination of femoral-tibial contact positions under in vivo conditions using fluoroscopy. Clinical Biomechanics 13, 455–472.

Jong, F.W.D., 1997. Mechanical analysis of hydroxyl-apatite coated knee prosthesis. Thesis, Technical University, Eindhoven, the Netherlands.

Kärrholm, J., 1989. Roentgen stereophotogrammetry. Review of orthopedic applications. Acta Orthopaedica Scandinavica 60, 491–503.

Lavallée, S., Szeliski, R., 1995. Recovering the position and orientation of free-form objects from image contours using 3D distance maps. IEEE Transactions on PAMI 17, 378–390.

Lowe, D.G., 1987. Three-dimensional object recognition from single two-dimensional images. Artificial Intelligence 31, 355–395.

Nagels, J., Valstar, E.R., Stokdijk, M., Rozing, P.M., 2002. Patterns of glenoid component loosening. Journal of Bone and Joint Surgery [British] 84, 83–87.

Nelissen, R.G., Valstar, E.R., Rozing, P.M., 1998. The effect of hydroxyapatite on the micromotion of total knee prostheses. A prospective, randomized, double-blind study. Journal of Bone and Joint Surgery [American] 80, 1665–1672.

Ryd, L., 1992. Roentgen stereophotogrammetric analysis of prosthetic fixation in the hip and knee joint. Clinical Orthopaedics 56–65.

Sarojak, M., Hoff, W., Komistek, R., Dennis, D., 1999. An interactive system for kinematic analysis of artificial joint implants. Biomedical Sciences Instrumentation 35, 9–14.

Selvik, G., 1989. Roentgen stereophotogrammetry. A method for the study of the kinematics of the skeletal system. Acta Orthopaedica Scandinavica Supplementum 232, 1–51.

Spellucci, P., 1998. An sqp method for general nonlinear programs using only equality constrained subproblems. Mathematical Programming 82, 413–448.

Vrooman, H.A., Valstar, E.R., Brand, G.J., Admiraal, D.R., Rozing, P.M., Reiber, J.H., 1998. Fast and accurate automated measurements in digitized stereophotogrammetric radiographs. Journal of Biomechanics 31, 491–498.

Valstar, E.R., Vrooman, H.A., Toksvig-Larsen, S., Ryd, L., Nelissen, R.G., 2000. Digital automated RSA compared to manually operated RSA. Journal of Biomechanics 33, 1593–1599.

Valstar, E.R., Jong, F.W.D., Vrooman, H.A., Rozing, P.M., Reiber, J.H.C., 2001. Model-based roentgen stereophotogrammetry of orthopaedic implants. Journal of Biomechanics 34, 715–722.

Valstar, E.R., Garling, E.H., Rozing, P.M., 2002. Micromotion of the Souter-Stratchclyde total elbow prosthesis in patients with rheumatoid arthritis. Acta Orthopaedica Scandinavica 73, 264–272.

Wunsch, P., Hirzinger, G., 1996. Registration of CAD-Models to Images by Iterative Inverse Perspective Matching. Vienna, Austria, pp. 77–83.

Zuffi, S., Leardini, A., Catani, F., Fantozzi, S., Cappello, A., 1999. A model-based method for the reconstruction of total knee replacement kinematics. IEEE Transactions on Medical Imaging 18, 981–991.